Asteroseismic estimate of helium abundance of a solar analog binary system

Kuldeep Verma[1], João P. Faria[2,3], H. M. Antia[1], Sarbani Basu[4], Anwesh Mazumdar[5], Mário J. P. F. G. Monteiro[2,3], Thierry Appourchaux[6], William J. Chaplin[7,8], Rafael A. García[9], Travis S. Metcalfe[10,8]

Received _____; accepted _____

[1]Tata Institute of Fundamental Research, Homi Bhabha Road, Mumbai 400005, India

[2]Centro de Astrofísica da Universidade do Porto, Rua das Estrelas, 4150-762 Porto, Portugal

[3]Departamento de Física e Astronomia, Faculdade de Ciências da Universidade do Porto, Rua do Campo Alegre, 4169-007 Porto, Portugal

[4]Astronomy Department, Yale University, P. O. Box 208101, New Haven, CT 065208101, USA

[5]Homi Bhabha Centre for Science Education, TIFR, V. N. Purav Marg, Mankhurd, Mumbai 400088, India

[6]Institut d'Astrophysique Spatiale, Université Paris XI-CNRS (UMR8617), Batiment 121, F-91405 Orsay Cedex, France

[7]School of Physics and Astronomy, University of Birmingham, B15 2TT, UK

[8]Stellar Astrophysics Centre, Department of Physics and Astronomy, Aarhus University, Ny Munkegade 120, DK-8000 Aarhus C, Denmark

[9]Laboratoire AIM, CEA/DSM, CNRS, Université Paris Diderot, IRFU/SAp, Centre de Saclay, 91191 Gif-sur-Yvette Cedex, France

[10]Space Science Institute, Boulder, CO 80301, USA

ABSTRACT

16 Cyg A and B are among the brightest stars observed by *Kepler*. What makes these stars more interesting is that they are solar analogs. 16 Cyg A and B exhibit solar-like oscillations. In this work we use oscillation frequencies obtained using 2.5 years of *Kepler* data to determine the current helium abundance of these stars. For this we use the fact that the helium ionization zone leaves a signature on the oscillation frequencies and that this signature can be calibrated to determine the helium abundance of that layer. By calibrating the signature of the helium ionization zone against models of known helium abundance, the helium abundance in the envelope of 16 Cyg A is found to lie in the range 0.231 to 0.251 and that of 16 Cyg B lies in the range 0.218 to 0.266.

Subject headings: stars: individual: HD 186408, HD 186427; stars: abundances; stars: interiors; stars: oscillations; stars: solar-type

1. Introduction

Helium is the second most abundant element in normal stars and has a pronounced effect on their structure and evolution. Unfortunately, helium abundance cannot be determined spectroscopically for low-mass stars because of their low temperatures. As a result, the initial helium abundance of stellar models depends on an assumption about galactic chemical evolution. For instance, the Yale-Yonsei Isochrones (Demarque et al. 2004) were constructed assuming $Y_0 = 0.23 + 2Z_0$, Y_0 and Z_0 being respectively the initial helium and heavy-element abundances. The Dartmouth tracks (Dotter et al. 2008) assume $Y_0 = 0.245 + 1.54Z_0$, while the Padova tracks of Marigo et al. (2008) assume $Y_0 = 0.23 + 2.23Z_0$. Such ad hoc prescriptions could easily lead to large errors in results for single stars that are determined using such sets of isochrones and tracks.

When additional data, such as frequencies of stellar oscillations and other spectroscopically determined stellar parameters are available, the helium abundance is often treated as one of the free parameters that are adjusted to obtain the best fit to the data (see e.g., Metcalfe et al. 2010, 2012; Mathur et al. 2012; Gruberbauer et al. 2013, etc). While such methods give better constraints on the initial helium abundance, there are possible systematic errors that are introduced because of our inability to model the near surface layers of a star properly. Normal one-dimensional models treat convection only in gross approximations and do not treat the dynamical effects of convection at all. This leads to large differences in the structure of the near surface layers that introduces a frequency-dependent error in the frequencies (see, e.g., Christensen-Dalsgaard & Berthomieu 1991) that is usually referred to as the "surface effect". Removal of the surface effect can introduce errors in the determined stellar properties.

There are however, more direct ways of determining the helium abundance of a star using its oscillation frequencies. The process of ionization of helium locally depresses the

adiabatic index, Γ_1, which in turn affects the sound speed in that region, and consequently, the frequencies of acoustic modes. In the case of the Sun, the signature that helium ionization leaves on the sound-speed profile has been used successfully to determine the helium abundance in the solar convection zone (e.g., Basu & Antia 1995, and references therein). For the Sun, the helioseismic estimation of helium abundance was facilitated by the fact that the frequencies of about a few thousand modes of degrees ranging from $l = 0$ (the radial mode) to $l = 250$ have been determined precisely. This is not the case for other stars, where only modes of $l = 0$–2 and sometimes $l = 3$ can be determined. Thus the estimation of helium abundance has to be done with a different technique.

To estimate the helium abundance in other stars, one can exploit the fact that the steep variation in the sound speed in the second helium ionization zone introduces an oscillatory component, $\delta\nu$, in the oscillation frequencies as a function of the radial order, n, of the modes (Gough & Thompson 1988; Vorontsov 1988; Gough 1990). The signal varies as $\sin(4\pi\tau_{\rm He}\nu + \phi)$, where $\tau_{\rm He}$ is the acoustic depth of the ionization layer as measured from the stellar surface, i.e.,

$$\tau_{\rm He} = \int_{r_{\rm He}}^{R_*} \frac{dr}{c} \,, \tag{1}$$

c is the sound speed, $r_{\rm He}$ the radial distance to the ionization layer, R_* is the stellar radius, $\nu = \nu_{n,l}$ is the frequency of a mode with radial order n and degree l, and ϕ is the phase of the oscillatory term. The amplitude of the signal is predominantly a function of the helium abundance — higher the abundance, higher the amplitude; but there is also an effect of mass, effective temperature, and luminosity, which is why it is important to choose close enough calibrating models. Basu et al. (2004), Houdek (2004), and Monteiro & Thompson (2005) explored theoretically how this signature may be used to determine the helium abundance of other stars. While thus far no one has used this signature to determine the helium abundance of any star other than the Sun, it has been used to determine the acoustic depth of the helium ionization zone. Using data from *CoRoT*, Miglio et al. (2010)

determined the location of the second helium ionization zone for the red giant HR 7349, they lacked sufficient signal to noise to determine the helium abundance. Again using *CoRoT* data, Roxburgh (2011) and Mazumdar et al. (2011, 2012) determined the position of the HeII ionization zone of the solar-type star HD 49933. Mazumdar et al. (2014) have extended this study to 19 stars observed by *Kepler*. Note that a similar oscillatory signature, but at a larger acoustic depth $\tau_{\rm CZ}$ arises from the discontinuity in the **second derivative of the sound speed** at the base of the convection zone and can be used to determine the depth of the convection zone (Ballot et al. 2004; Mazumdar 2005; Piau et al. 2005).

In this work we determine the helium abundance in 16 Cyg A and B (HD 186408 and 186427; KIC 12069424 and 12069449) using oscillation frequencies determined from 2.5-years of observations by the *Kepler* satellite. These stars form a binary system and are among the brightest stars in the *Kepler* field of view. Analysis of a three month time series to constrain the properties of the stars have shown that the stars are slightly more massive than the Sun and somewhat older too. Using the frequencies of oscillations, along with spectroscopic constraints on the effective temperature and metallicity of the stars, Metcalfe et al. (2012) found the stars to be 6.8 ± 0.4 Gyr old with an initial composition to be $Z_0 = 0.024 \pm 0.002$ and $Y_0 = 0.25 \pm 0.01$. They estimated the masses of the A and B components to be $1.11 \pm 0.02\ M_\odot$ and $1.07 \pm 0.02\ M_\odot$, respectively. Using similar technique Gruberbauer et al. (2013) found a somewhat larger helium abundances for these stars. However, these values of helium abundance depend on input physics of stellar models and on how the surface effects are corrected for. A more direct determination of the current helium abundance in the envelope, Y, is thus in order.

The rest of the paper is organized as follows. We describe the methods we have used to determine the helium abundance from the signature of the ionization zone in Section 2,

the models used for the calibration of the helium signature are described in Section 3, the results are presented in Section 4 and we discuss the results in Section 5.

2. Extracting the helium signal from the data

The amplitude of the oscillatory term, introduced by the localized depression of Γ_1 in the helium ionization zone, is quite small, and different techniques have been used to extract this signal. In this work we use three techniques, the first (Method A) relies on taking the second differences of the frequencies of a given degree with respect to the radial order n to suppress the smooth variation in frequencies. The other two methods (Methods B and C) rely on directly fitting the oscillatory signature while simultaneously modelling the predominantly smooth behavior of the frequencies as a function of n. The difference between the Methods B and C is in the form of oscillatory function used in fitting and how the smooth component is adjusted. We describe these methods in more detail below.

2.1. Technique using second differences (Method A)

To extract the oscillatory signal from the frequencies we take the second difference (Gough 1990; Basu et al. 1994, 2004) of the frequencies with respect to the radial order n, i.e.,

$$\delta^2\nu_{n,l} = \nu_{n-1,l} - 2\nu_{n,l} + \nu_{n+1,l}. \tag{2}$$

The advantage of taking the second difference is that the contribution from the smooth variation of the frequencies with n is greatly reduced since the dominant variation of ν with n is linear.

We fit the second differences to a suitable functional form that represents the oscillatory signal from the HeII ionization zone as well as that from the base of the convection zone

(Mazumdar & Antia 2001). For this purpose we use the following form which has been adapted from Houdek & Gough (2007)

$$\begin{aligned}\delta^2\nu &= a_0 + a_1\nu + \frac{b_2}{\nu^2}\sin(4\pi\nu\tau_{\rm CZ} + \psi_{\rm CZ}) \\ &\quad + c_0\nu\, e^{-c_2\nu^2}\, \sin(4\pi\nu\tau_{\rm He} + \psi_{\rm He}),\end{aligned} \tag{3}$$

where $a_0, a_1, b_2, c_0, c_2, \tau_{\rm CZ}, \tau_{\rm He}, \psi_{\rm CZ}, \psi_{\rm He}$ are free parameters which are fit to the observed second differences. In Eq. (3) the first two terms represent the smooth part of the function, which remains after the second differences are calculated and includes a contribution from the hydrogen and first helium ionization zone; the third term represents the contribution from the base of the convection zone, while the last term represents the contribution from the HeII ionization zone. **It is possible to add more terms to the smooth part using a higher degree polynomial, but for both stars considered in this work, the reduction in χ^2 due to additional terms was found to be statistically insignificant; the linear term was found to have a significant effect. Hence, we have restricted the smooth part to linear form in this work.**

The parameters of Eq. (3) are determined by a nonlinear least-squares fit. Since the second differences of a given value of l and neighboring n have correlated errors, we use the full covariance matrix to calculate the value of χ^2. We assume that the errors in the frequencies themselves are not correlated with each other to obtain the covariance matrix. Since the nonlinear minimization does not always converge to the global minimum of the parameter space, we repeat the minimization 100 times with different initial guesses which are randomly selected in some range of possible values. The minimum of the χ^2 values obtained for the 100 trials is accepted as the best fit value.

To estimate the uncertainties in the fitted parameters we repeat the whole process for 1000 realizations of the data obtained by adding random perturbations to the frequencies with standard deviation equal to 1σ uncertainty in the corresponding frequencies. The

median value of each parameter for 1000 realizations was accepted as the fitted value, while the $\pm 1\sigma$ uncertainty in the fitted value was estimated from the range covering 34% area on either side of the median in the distribution function of the fitted parameter. For the two stars being analyzed we find that while the signal from HeII ionization zone is robust and all realizations of the data result in values of $\tau_{\rm He}$ in a reasonable range, the distribution of the fitted values of $\tau_{\rm CZ}$ is extremely wide with multiple peaks. We find that the oscillatory signal from the base of the convection zone is weak for both 16 Cyg A and B. For some of the realizations we find that fitting $\tau_{\rm CZ}$ is difficult. An analysis of the peaks reveals that one of the secondary peaks corresponds to $\tau = T_0 - \tau_{\rm CZ}$ where T_0 is the acoustic radius of the star. This can happen due to aliasing (Mazumdar & Antia 2001). We discard all realizations for which the fitted value of $\tau_{\rm CZ}$ does not lie in the dominant peak of the distribution of $\tau_{\rm CZ}$. The median of the dominant peak is used as the estimate for $\tau_{\rm CZ}$. For determining other fitted parameters too we use only those realizations that have $\tau_{\rm CZ}$ in the dominant peak. Note that this paper is about determining the helium abundance of these stars, and not the position of the convection-zone base, though that is by itself an interesting question. To this effect we have tested whether our inability to fit $\tau_{\rm CZ}$ reliably affects the helium results by fixing the value of $\tau_{\rm CZ}$ at different values around the main peak. The fit to the HeII signal is unaffected, and therefore we are certain that our results concerning helium are not biased.

The amplitude of the helium signal in the second differences can be converted to that in the frequencies by dividing the second-difference amplitude by a factor $4\sin^2(2\pi\tau_{\rm He}\Delta_0)$, where $\tau_{\rm He}$ and Δ_0 are the acoustic depth and the average large frequency separation respectively. **This factor is derived under the assumption that the amplitude of oscillatory signal varies slowly over the 'wavelength' of oscillation.** The amplitude of the oscillatory signal depends on the helium abundance in the ionization zone which in stars that have an outer convection zone is the helium abundance of the convective envelope.

As shown by Basu et al. (2004), the amplitude of the signal can be calibrated using models with known helium abundance. Basu et al. (2004) used the average amplitude over the frequency interval that is used in fitting the signal to measure the helium abundance; we do the same.

2.2. Technique using frequencies directly (Method B)

To extract directly the signal from the oscillation frequencies, we adapt a method first proposed by Monteiro et al. (1994). The approach is, first, to fit a smooth function of radial order n to all the modes $\nu_{n,l}$ of same degree l, which removes the slowly varying trend. For each degree l, we fit a polynomial $P_{l,\mathrm{B}}(n)$ using least-squares method with third derivative smoothing. The resulting smooth function removes mainly variation of $\nu_{n,l}$ at much longer scales than the characteristic scales of the oscillatory signals, filtering out the signatures of the acoustic glitches. The filtered signal is then fitted simultaneously for all degrees to the following expression;

$$\begin{aligned} \delta\nu &= A_{\mathrm{CZ}} \left(\frac{\nu_r}{\nu}\right)^2 \cos\left(4\pi\tau_{\mathrm{CZ}}\nu + \phi_{\mathrm{CZ}}\right) \\ &\quad + A_{\mathrm{He}} \left(\frac{\nu_r}{\nu}\right) \sin^2(2\pi\beta_{\mathrm{He}}\nu) \cos\left(4\pi\tau_{\mathrm{He}}\nu + \phi_{\mathrm{He}}\right), \end{aligned} \tag{4}$$

where A_{CZ}, τ_{CZ}, ϕ_{CZ}, A_{He}, β_{He}, τ_{He}, ϕ_{He} are 7 free parameters, while ν_r is a reference frequency.

We have used a modified version of the method used in previous works (Monteiro et al. 1994; Monteiro & Thompson 1998; Monteiro et al. 2000). It differs mainly in three aspects: (1) a global minimization method, based on the PIKAIA implementation of a genetic algorithm (Charbonneau 1995), is used for the least-squares fit providing independence of initial conditions; (2) the robustness of the fit against outliers is improved by performing an iteratively reweighted least-squares regression (e.g., Street et al. 1988); and (3) both signals

from the base of the convection zone and the HeII ionization zone are fitted simultaneously.

The third derivative smoothing procedure depends on a parameter $\lambda_{\rm B}$ which determines how closely the polynomial $P_{l,{\rm B}}(n)$ interpolates the points (Monteiro et al. 1994, their Eq. C5). Here, we no longer iterate on this parameter but set it to a value adequate for isolating the longest period signal from the HeII ionization zone. The same value of $\lambda_{\rm B}$ is used for both stars, either observations or model frequencies. With this method, all available data points are used (frequencies of consecutive orders are not required to construct combinations) and we do not *a priori* assume a specific functional form for the smooth component.

To estimate the uncertainties in the fitted parameters we perform 5000 Monte Carlo realizations of the frequencies by adding random perturbations to them with standard deviation equal to 1σ uncertainty in the corresponding frequencies. The median value of the distribution of each parameter was accepted as the fitted value and the $\pm1\sigma$ uncertainty in that parameter was estimated from the standard deviation of the distribution.

To calibrate the helium abundance, we used the amplitude of the signal at a reference frequency ν_r (= 2.0 mHz) for both components. This choice provides us a simple measure of the amplitude, $A_{\rm He}\sin^2(2\pi\beta_{\rm He}\nu_r)$ (see Eq. 4), and hence a measure of the amount of helium present in the ionization zone.

2.3. Technique using frequencies directly (Method C)

This technique is a modification of the previous one in the sense that it fits smooth and oscillatory signal together. For each l, we take a fourth degree polynomial in n, $P_{l,{\rm C}}(n)$, for the smooth component. Although, a third degree polynomial takes care of smooth component for the observed data, it is not enough for the models, as the surface

term introduces a smooth component which varies approximately as fourth power of the frequency (Kjeldsen et al. 2008). We fit directly the frequencies to the function;

$$\begin{aligned} f(n,l) &= P_{l,\mathrm{C}}(n) + \frac{A_{\mathrm{CZ}}}{\nu^2}\sin(4\pi\tau_{\mathrm{CZ}}\nu + \phi_{\mathrm{CZ}}) \\ &\quad + A_{\mathrm{He}}\nu e^{-c_2\nu^2}\sin(4\pi\tau_{\mathrm{He}}\nu + \phi_{\mathrm{He}})\,, \end{aligned} \tag{5}$$

where $P_{l,\mathrm{C}}(n) = \sum_{i=0}^{4} A_{l,i} n^i$. The 4×5 elements of $[A]_{l,i}$ along with A_{CZ}, τ_{CZ}, ϕ_{CZ}, A_{He}, c_2, τ_{He}, ϕ_{He} are 27 free parameters which need to be determined.

The parameters of Eq. (5) are determined by minimizing a χ^2 defined as;

$$\chi^2 = \sum_{n,l}\left[\frac{\nu_{n,l} - f(n,l)}{\sigma_{n,l}}\right]^2 + \lambda_{\mathrm{C}}^2 \sum_{n,l}\left[\frac{d^2 P_{l,\mathrm{C}}(n)}{dn^2}\right]^2\,, \tag{6}$$

where $\sigma_{n,l}$ is the uncertainty in the mode frequency and λ_{C} is a smoothing parameter. A very small value of λ_{C} corresponds to the standard weighted least-squares fitting, while a very large value tends to fit the frequencies to a straight line. To make an appropriate choice of λ_{C}, we note that as λ_{C} increases, the fit to the observation stabilizes (uncertainty in the fitting parameters decreases) and saturates at some point. We accept a value of λ_{C} when the stabilization occurs. The value of λ_{C} is found to be the same for both stars. To avoid systematic errors in the calibration, we use the same λ_{C} for the models as well. **While the number of parameters to be fitted in this method is large, it should be noted that the use of regularization introduces additional constraints that enable more parameters to be determined.**

Similar to what has been done in Method A, we repeat the minimization 100 times with random initial guesses covering a reasonable parameter space to get the global minimum. We simulate 1000 realizations of the data in the same way as was done in Method A to get the fitted value along with $\pm 1\sigma$ uncertainty. We calculate an average amplitude over the frequency range used in the fitting for the calibration.

3. Stellar models for calibration

To determine the helium abundance of the stars we need to compare the observed amplitudes of the helium signal to that calculated for stellar models with different helium abundances. We used three sets of models: two constructed with the MESA code (Paxton et al. 2011) for two different metallicity mixture, and one with the Yale stellar evolution code (YREC; Demarque et al. 2008). The models in each set were constructed following different principles and the models for calibration were selected using different criteria. The models and the selection process are described below.

3.1. The MESA models

The MESA code allows users to explore different input physics and data. Our models were constructed using OPAL equation of state (Rogers & Nayfonov 2002). We used OP opacities (Badnell et al. 2005; Seaton 2005) for models with metallicity mixture of Grevesse & Sauval (1998) (hereinafter GS98) and OPAL opacities for models with metallicity mixture of Asplund et al. (2009) (hereinafter AGSS09). Low temperature opacities were used from Ferguson et al. (2005) assuming GS98 mixture. Reaction rates from NACRE (Angulo et al. 1999) were used for all reactions except ^{14}N(p,γ)^{15}O and ^{12}C(α,γ)^{16}O, for which updated rates of reaction from Imbriani et al. (2005) and Kunz et al. (2002) were used. Convection was modelled using the standard mixing length theory (Cox & Giuli 1968), and diffusion of helium and heavy elements was incorporated using the prescription of Thoul et al. (1994).

We constructed models assuming two different values of the solar metallicity to convert the observed [Fe/H] to Z needed for the models. Recall that there is currently an uncertainty about what the solar metallicity really is. The solar abundances of GS98, with $Z/X = 0.023$, had been used extensively for many years and solar models constructed

with these abundances satisfied helioseismic constraints quite well (see e.g., Basu & Antia 2008). However, Asplund et al. (2005) redetermined the solar abundances using 3D model atmospheres and incorporating NLTE corrections for many lines and claimed that the solar abundance of heavy elements was much lower, $Z/X = 0.0165$. The relative abundances of different elements were also changed. Asplund et al. (2009) revised the abundances further to $Z/X = 0.018$. The lower abundances are not consistent with helioseismic constraints **(see e.g., Turck-Chièze et al. 2004; Bahcall et al. 2005, 2006; Delahaye & Pinsonneault 2006; Basu & Antia 2008; Christensen-Dalsgaard et al. 2009; Basu & Antia 2013)** and this discrepancy has not been resolved. To estimate the effect of this uncertainty on stellar models we used both GS98 and AGSS09 mixtures of heavy elements in this work. Opacities were calculated assuming the different heavy-element mixtures, and Z for the models were derived for a given [Fe/H] assuming that [Fe/H] = 0 corresponds to $Z/X = 0.023$ for the GS98 mixture and $Z/X = 0.018$ for the AGSS09 mixture.

We constructed models on a uniform grid of stellar parameters (mass M, initial helium abundance Y_0, initial metallicity $[\mathrm{Fe/H}]_0$, and mixing length parameter α) for both stars with two different metallicity mixtures, GS98 and AGSS09. The range of values in the grid for these parameters were: $M : 0.91-1.17\,M_\odot$, $Y_0 : 0.22-0.35$, $[\mathrm{Fe/H}]_0 : 0.12-0.26$, $\alpha : 1.9-2.3$. The step sizes were $0.02\,M_\odot$, 0.02, 0.02 dex and 0.05, respectively. A reduced χ^2 between the frequencies of the model ($\nu_{\rm mod}$, corrected for the surface term as per the formulation of Kjeldsen et al. (2008)) and the observed frequencies ($\nu_{\rm obs}$) is defined as;

$$\chi^2_\nu = \frac{1}{N}\sum_i \left(\frac{\nu_{\rm obs}-\nu_{\rm mod}}{\sigma_{\rm obs}}\right)^2_i , \qquad (7)$$

where $\sigma_{\rm obs}$ is the 1σ uncertainty in the observed frequency and the sum runs over $N = 12$ radial modes of the concerned star. A model with a particular M, Y_0, Z_0, and α is selected as an acceptable model of the star only if the evolutionary track enters in a 4-dimensional box formed by the 2σ uncertainties in the observed effective temperature, luminosity,

surface [Fe/H], and large separation as given in Table 1. Further degeneracy in the age is lifted by minimizing the χ^2_ν (Eq. 7). In other words, the "best" model on each evolutionary track is chosen through a matching of the frequencies, provided the parameters mentioned above agree within very conservative limits. The surface metallicity given by Ramírez et al. (2009), 0.096 ± 0.026 dex for 16 Cyg A and 0.052 ± 0.021 dex for 16 Cyg B, is not quite the same for both components. However, since the metallicities are quite similar, we assume the metallicity of the two stars to be equal, 0.096 ± 0.040 dex, with increased uncertainty. This may be justified as the stars form a binary system and hence their initial metallicities should be the same. Since we use multiple values of initial conditions M, Y_0, Z_0, α, we get two ensembles each, corresponding to the two abundance choices of GS98 and AGSS09, for 16 Cyg A and 16 Cyg B. These are not, however, the final sets of calibration models. The dispersion in the age of the models in each of these ensembles is nearly 5 Gyr. We use a further selection procedure described below which takes into account the fact that 16 Cyg A and B should have the same age. Models constructed with the AGSS09 mixture are treated separately from those constructed with the GS98 mixture so that the effect of the uncertainty in the solar metallicity on our results can be quantified.

We constrain the ages using the small frequency separation ($d_{l\,l+2}(n) = \nu_{n,l} - \nu_{n-1,l+2}$), which is known to be a good indicator of the evolutionary stage of main sequence stars (see e.g., Christensen-Dalsgaard & Frandsen 1988). We use the weighted average of the small separation over 12 pairs, $\langle d_{02} \rangle$, for both components. However, we do not select the models with $\langle d_{02} \rangle$ alone, but consider other observables — namely, the effective temperature ($T_{\rm eff}$), luminosity (L), surface gravity (as $\log g$), surface metallicity (as [Fe/H]), and the large separation (Δ_0) — as well. Although, the radii of the two components have been measured with interferometry (White et al. 2013), we do not use the radii to constrain the ages, but it should be noted that the interferometric radii are found to be consistent with the final model radii for both stars.

We estimate the average large frequency separation ($\Delta_0 = \langle \nu_{n,0} - \nu_{n-1,0} \rangle$) of the radial modes by using a linear fit to the frequencies $\nu_{n,0}$ as a function of n. The same 12 radial modes are used that were used for calculating the average small separation. The same set of modes are used to calculate the average large separation for the observation and the models. As mentioned earlier, the inadequacy of modelling the near-surface layers of the star introduces a frequency-dependent shift in the calculated eigenfrequencies, $\nu_{n,l}$ of the models, making the frequencies systematically larger than observed frequencies for all but the lowest-frequency modes. This error propagates into the large separation too. We find that for our acceptable models Δ_0 is about 1μHz larger than the observed value. We estimated the exact shift using the differential form of the Duvall Law, as formulated by Christensen-Dalsgaard et al. (1989), in which the frequency differences between a model and observation are decomposed into two parts, one that depends on the interior structural differences and another that is essentially the surface term. The Δ_0 values of the model are corrected for the surface term before comparing them to the observed values of 16 Cyg A and B.

We estimated independently the age of 16 Cyg A and 16 Cyg B using models of two different metallicity mixture. To estimate the age of a star using models of a particular metallicity mixture, we define a χ^2 for each model as:

$$\chi^2_{\rm ind} = \sum_q \frac{(q_{\rm mod} - q_{\rm obs})^2}{\sigma_q^2} + \frac{(t_{\rm mod} - t_{0,\rm ind})^2}{\sigma_t^2}. \qquad (8)$$

The term q in the summation represents 6 observable quantities (Δ_0, $\langle d_{02} \rangle$, $T_{\rm eff}$, L, $\log g$, and [Fe/H]) and σ_q denotes the uncertainty in the estimate of the respective quantity. The quantity $t_{\rm mod}$ is the age of the model under consideration and $t_{0,\rm ind}$ is a reference age. For a given $t_{0,\rm ind}$, we can find a model that represents the star most closely by minimizing the $\chi^2_{\rm ind}$ (Eq. 8) over all the models in the ensemble. We denote the minimum by $\chi^2_{\rm min}$, and minimize it with respect to $t_{0,\rm ind}$ in a range spanned by the model ages in the ensemble, to

get the individual age of the star. For clarity we show the $\chi^2_{\rm min}$ in Fig. 1(a) in a limited range of $t_{0,\rm ind}$. Clearly the curves have a well defined minimum that gives the best model as well as the best estimate of the age of each individual star for a specific assumed metallicity mixture. The ages are respectively 6.9 ± 0.4 Gyr and 6.6 ± 0.4 Gyr for 16 Cyg A and B when GS98 mixture is used. For the AGSS09 mixture the ages are respectively 7.1 ± 0.4 Gyr and 6.7 ± 0.4 Gyr. Thus the ages of the two stars are found to be close to each other and the values are consistent with those of Metcalfe et al. (2012) and Gruberbauer et al. (2013). Note that the calculation of $\chi^2_{\rm ind}$ requires σ_t; we start with a suitable guess and then whole process is iterated until we get the same uncertainty in the estimated age as σ_t.

The individual ages of the two stars, independently determined as explained above, need not turn out to be the same. However, since the stars form a binary system it is more natural to assume that their ages are the same. We can determine this common age by modifying the definition of χ^2 to include both stars. Thus for a given pair of models, with one model drawn from the model ensemble of 16 Cyg A and the other from that of the 16 Cyg B, we define a combined χ^2 as:

$$\begin{aligned} \chi^2_{\rm com} &= \sum_{q_{\rm A}} \frac{(q_{\rm A,mod} - q_{\rm A,obs})^2}{\sigma^2_{q_{\rm A}}} + \frac{(t_{\rm A,mod} - t_{0,\rm com})^2}{\sigma^2_t} \\ &+ \sum_{q_{\rm B}} \frac{(q_{\rm B,mod} - q_{\rm B,obs})^2}{\sigma^2_{q_{\rm B}}} + \frac{(t_{\rm B,mod} - t_{0,\rm com})^2}{\sigma^2_t}. \end{aligned} \tag{9}$$

The first two terms correspond to the model of the A component while the last two correspond to the model of the B component. The summations in the first and third terms again have 6 terms each corresponding to the same observables as described above. The quantities $t_{\rm A,mod}$ and $t_{\rm B,mod}$ are the ages of the models of 16 Cyg A and 16 Cyg B under consideration. The quantity $t_{0,\rm com}$ is a reference age as before, but common to both stars. For a given $t_{0,\rm com}$, we can find a pair of models that represents the stars most closely by minimizing the $\chi^2_{\rm com}$ (Eq. 9) over all possible pairs of the two ensembles. We denote the minimum by $\chi^2_{\rm min}$, and minimize it with respect to $t_{0,\rm com}$ in a range spanned by the model

ages in the two ensemble, to get the common age of the star. For clarity we show the $\chi^2_{\rm min}$ in Fig. 1(b) in a limited range of $t_{0,\rm com}$. Again, the resulting curves have a well defined minimum that gives the best pair of models as well as the best estimate of the common age of the stars. The individual models of such a pair are essentially the best models of 16 Cyg A and B. The age of the binary system is estimated to be 6.7 ± 0.3 Gyr for GS98 mixture, and 6.9 ± 0.3 Gyr for AGSS09 mixture. Thus we find that the mixture of heavy elements does not affect the age significantly. **The difference in the age between models of two mixtures may become significant when the stellar parameters and the oscillation frequencies are known more precisely. Houdek & Gough (2011) have pointed out that along with d_{02} we can use coefficients of higher order asymptotic formula for oscillation frequency to determine the age more precisely as these are more sensitive to the sound speed variation in the stellar core. However, it is not clear if these terms can be determined more accurately from the currently observed frequencies.**

At the end of this selection procedure we are left with approximately 450 models, nearly 100 models for a star with a particular metallicity mixture, with a range of mass, chemical composition, and mixing length parameters, and age within 1σ of the value determined above. For the two metallicity mixtures, GS98 and AGSS09, we have two such set of calibrating models.

3.2. The YREC models

In addition to the models described above, we also used the Yale stellar evolution code to model the two stars. The input physics includes the OPAL equation of state (EOS) tables of Rogers & Nayfonov (2002), and OPAL high temperature opacities (Iglesias & Rogers 1996) supplemented with low temperature opacities from Ferguson et al. (2005). All nuclear

reaction rates are from Adelberger et al. (1998), except for that of the $^{14}N(p,\gamma)^{15}O$ reaction, for which we use the rate of Formicola et al. (2004). All models included gravitational settling of helium and heavy elements using the formulation of Thoul et al. (1994). Models were constructed assuming the heavy element mixture of GS98.

The YREC models were constructed with an approach that was quite different from the MESA models. The starting point of the modelling was the mass and radius of the two stars as determined by Metcalfe et al. (2012). We did a Monte Carlo around this mass and radius, and the spectroscopically determined $T_{\rm eff}$ and metallicity to obtain a set of values for mass, final radius, final $T_{\rm eff}$ and final metallicity. YREC was used in an iterative mode. In this mode the final $T_{\rm eff}$ and radius for a star of a given mass and metallicity are specified. The code iterates over the initial helium abundance Y_0 in case the mixing length parameter α is specified, or alternatively over α if Y_0 is specified until a model with the specified $T_{\rm eff}$ and radius is found. Note that this is similar to the construction of standard solar models, though in the case of the Sun the iteration is performed simultaneously over both mixing length parameter and Y_0 (since the solar age is a known constraint). We made the models both ways — specifying α and determining Y_0 and specifying Y_0 and determining α. The initial metallicity of the models was kept higher than the observed metallicity in order to account for the depletion of metals by diffusion. The Monte Carlo exercise assumed that the width of the distribution in mass and radius was three times the quoted uncertainty in Metcalfe et al. (2012). These models, by construction, satisfy the temperature constraint. Models of 16 Cyg A and B were constructed independently.

The final selection of models was done as follows. All models with initial helium abundance lower than the Big Bang nucleosynthesis value of $Y_p = 0.2477$ (Peimbert et al. 2007) were rejected. Also rejected were models with final metallicities that were different from the observed metallicity (Ramírez et al. 2009) by more than 3σ. We calculated the

frequencies for the remaining models. The frequencies were used to calculate the frequency ratios r_{02}, r_{10}, and r_{01} (Roxburgh & Vorontsov 2003; Silva Aguirre et al. 2011). These ratios are insensitive to the surface term and hence do not require any *ad hoc* corrections to account for near-surface uncertainties in the models. All models that matched the observed ratios to within 3σ were selected. The common age of the 16 Cyg system was estimated to be 6.6 ± 0.3 Gyr in the same way as described in Section 3.1. This resulted in 231 models for 16 Cyg A and 95 models for 16 Cyg B for calibration after applying the age constraint.

4. Results

We applied all three techniques described in Section 2 to estimate the helium abundance of both components of the 16 Cyg system. We also estimated the acoustic depths of the HeII ionization zone and made preliminary estimates of the acoustic depths of the base of the convection zone.

In this work, we used observed frequencies computed following the procedure described by Appourchaux et al. (2012) from 2.5 years of *Kepler* simple-aperture-photometry light curves corrected following García et al. (2011) and high-pass filtered with a 4-days triangular smooth. The observed frequencies as used in this work are given in Table 2. All frequencies listed in the table were used in the fits except for the last two modes for 16 Cyg A which were not used in Methods A,C as these modes are beyond the cut-off frequency in many stellar models and hence cannot be determined reliably in stellar models which are used for calibration. The Method B is not expected to be sensitive to presence of these modes in the observed frequency set as the amplitude of helium signal is compared at a reference frequency instead of the average over entire range covered in the fit, which is the case in Methods A,C. Further, the two isolated $l = 3$ modes cannot be used in Method A, which needs to compute second order differences.

The upper panels of Fig. 2, 3, and 4 show respectively the fit to Eq. (3) (Method A), Eq. (4) (Method B) and Eq. (5) (Method C) of 16 Cyg A and B; whereas the lower panels show the histograms of distribution of $\tau_{\rm He}$ (blue) and $\tau_{\rm CZ}$ (red) obtained by fitting 1000 realizations (5000 for Method B) of data perturbed by adding random errors. The fitted values of the various physical parameters are listed in Table 3. It should be noted that for Methods A and C, the amplitude is averaged over the fitting interval, while for Method B, it is calculated at a reference frequency. **As explained in Section 2.1, the amplitude of oscillatory term in second differences is converted to that in frequencies. From the table it can be seen that the amplitudes of oscillatory signals obtained with methods A and C are similar. This demonstrates the validity of conversion factor. The fitted parameters using all three methods are close to each other and generally within 1σ, except for $\tau_{\rm He}$ using method B. Even in this case the difference is only about 6% of the acoustic depth. This demonstrates that the results are not particularly sensitive to different form of oscillatory term or to different techniques for removing the smooth component in the frequencies as a function of n.**

The frequencies for the models were fitted in the same manner, and using the same modes and weights as the observations. Amplitude of the HeII signal obtained using Method A is shown in Fig. 5 for each MESA model. Also shown in the figure is the observed amplitude. Note from the figure that the amplitude is predominantly a function of the current helium abundance in the models. There is however, some scatter due to other model parameters, primarily due to variations in mass, effective temperature, and luminosity. The helium abundance, Y, obtained by calibrating the model amplitude with observation are listed in Table 4 for both stars. The helium abundance obtained with MESA and YREC are consistent with each other within errors. There is a difference, barely within errors, between the helium abundance of 16 Cyg A and 16 Cyg B. For 16 Cyg A all 3 methods give

results that are within error bars of each other, but for 16 Cyg B Method A tends to give results that are on higher side, while Method B tends to give lower values. The difference between the two methods is up to 2.5σ. The difference in results between various methods can be considered to be a measure of systematic errors. **The estimate of Y doesn't directly depend on $\tau_{\rm He}$ and hence is not affected by uncertainties in it.**

The precision of determination of helium abundance depends critically on the modes at the low end of the spectrum. Addition of a few low order modes or any significant improvement in the precision of these modes, improve the precision of estimate of helium abundance significantly. To understand this improvement we repeated the fit using Method C after removing successively the lowest order modes, or after increasing the uncertainties in the lowest three modes of degree 0, 1, and 2. We found that the uncertainty in the amplitude of the helium signal increases rapidly in each case, by a factor of two or more. This may be due to the fact that the amplitude of the signal decreases very rapidly with increasing frequency, and the low order modes play a role in stabilizing the fit as in that region the amplitude of helium signal is larger. Therefore a precise determination of the helium abundance of a star would particularly require a precise set of low order modes.

In Method B, the amplitude of the oscillatory signal at a reference frequency (instead of the mean amplitude used in other methods) is used to calibrate the helium abundance. The stability of this approach has been tested by Monteiro & Thompson (2005) for the case of the Sun. They found that the use of a reference frequency well inside the frequency range of the observations was a better, more stable option, to calibrate Y. This is so because the approach used by this method to account for the smooth component is fairly robust in the inner region of the frequency range (does not change regardless of the details for smooth component that is adjusted). In this way, this method can avoid any

contamination from the boundaries due to the smoothing.

The oscillatory signal in the observed frequencies contains information about the location of the acoustic glitches. Fig. 6 shows the acoustic depths of the base of the convection zone and the HeII ionization zone obtained using all 3 methods. The τ for the models were estimated in two different ways; one by calculating the acoustic depth from the known sound-speed profile of the model (Eq. 1), and the other by fitting the second differences of the model frequencies (Eq. 3) or by fitting the model frequencies (Eq. 4 or 5). **The first estimate using Eq. 1, is affected by the uncertainties in the definition of stellar surface. This issue has been extensively discussed by Houdek & Gough (2007) and will affect the acoustic depth of all layers by the same amount. However, the uncertainties in τ do not affect the determination of Y which depends on the amplitude of the oscillatory signal.** As can be seen in the figure, for $\tau_{\rm CZ}$ the two estimates for a model match well, but for $\tau_{\rm He}$ the value obtained from Eq. (1) is systematically higher than that obtained by fitting the second differences or the frequencies. This systematic shift is present in the results of all the three fitting methods, and could be due to the fact that for $\tau_{\rm CZ}$ the location of the discontinuity in the sound-speed gradient is well-defined and there is little ambiguity in its position; for $\tau_{\rm He}$ on the other hand there is, strictly speaking, no real discontinuity at all, but merely a sharp variation in Γ_1 that gives rise to the oscillatory signal in the frequencies. While using Eq. (1) we used the minimum in Γ_1 in the HeII ionization zone as the location of the 'discontinuous' layer, and it is possible that the effective location of the 'discontinuity' is at a layer above this. The value of $\tau_{\rm CZ}$ obtained by fitting the observed frequencies is close to what we get for our models; $\tau_{\rm He}$ obtained from the observed frequencies lies within about 3σ of that obtained by fitting the frequencies of the models. The amplitude of signal due to the base of the convection zone in the observed frequencies is consistent with those in the models' frequencies.

We examined the variation of the average amplitude of the HeII signal with the input parameters of the models and their seismic characteristics. Fig. 7 shows the variation of the average amplitude calculated using the fitting Method A for 16 Cyg A. We can see that the average amplitude of the HeII signal is not particularly sensitive to the metallicity and mixing length parameter (see Fig. 7a, 7b); however, it shows systematic variation as a function of effective temperature, luminosity, large frequency separation, and **age** (see Fig. 7c-f). Much of the trend is essentially due to variation in Y with these parameters rather than variation of the amplitude for a given Y. The vertical dispersion in each of these figures is due to the dispersion in mass, which also changes Y at a given set of parameters. The variation of the amplitude was very similar when calculated using Method B and C.

5. Conclusions

We have used the oscillatory signature in the oscillation frequencies of 16 Cyg A and B caused by the depression of Γ_1 in the HeII ionization zone to determine the current helium abundance and the depth of the HeII ionization zone. For this task we have used frequencies obtained with 2.5 years of *Kepler* observations. We have used three different techniques combined with three sets of stellar models for calibrating the signal. We have demonstrated that the helium abundance of these stars can be reliably determined using the observed frequencies. For 16 Cyg A the three methods give results that are consistent with the error bars, while for 16 Cyg B the results can differ, though the difference is only 2.5σ in the worst case. The helium abundance for 16 Cyg A is found to lie in the range 0.231 to 0.251 and that of 16 Cyg B lies in the range 0.218 to 0.266.

The error bars quoted in Table 4 are the random errors arising from those in the observed frequencies. In addition, there would be systematic uncertainties due to approximate form of oscillatory term as well as uncertainties in the used

stellar models. The first contribution can be estimated from the differences in values obtained using the three techniques and is already included in the values quoted above. The stellar-model uncertainty should be mainly from the EOS which translates the helium abundance to Γ_1. From extensive tests for the Sun, it is known that the OPAL EOS is close to that of the Sun (see e.g. Basu & Christensen-Dalsgaard 1997) and hence we do not expect much uncertainty on that count in these stars where the uncertainties in the frequencies are much larger than those for the Sun.

This technique for determining helium abundance is not particularly sensitive to the presence of surface effect — the surface corrections are smooth function of n and will mainly contribute to the smooth part of the frequency and can be separated from the oscillatory part. This is particularly true when the observed frequencies are available over a wide range of n values as is the case with both stars considered here. If the observed frequency range is limited, there could be some difficulty in separating the helium signal from smooth part since the oscillatory signal can also be approximated with moderately high degree polynomial. This is the reason why we restrict the degree of polynomial in Method A to the minimum value that is statistically significant. The regularization used in Methods B and C allows us to use a more complex function to account for the smooth component.

The estimates of the helium mass fraction are those of the current abundance in the outer envelope of the stars. This value is, of course, lower than the initial helium abundance of both stars because of the gravitational settling of helium. We can determine the initial helium abundance from the current one by assuming that the models of the two stars correctly represent the amount of helium depleted due to settling. MESA models show a

depletion of 0.048 ± 0.004 (for GS98 mixture) and 0.054 ± 0.006 (for AGSS09 mixture) for 16 Cyg A. Depletion of helium is lesser for 16 Cyg B models, 0.043 ± 0.006 for GS98 and 0.048 ± 0.007 for AGSS09 mixture. Since the two components of the binary system are believed to have formed from the same gas cloud, the initial composition should be the same for both stars. In that case the current helium abundance in the envelope of 16 Cyg B should be higher than that in 16 Cyg A by about 0.005. The values that we find are consistent with this difference. This difference arises because of small difference in masses of the two stars. Similarly, the difference between GS98 and AGSS09 mixtures arise due to the difference in the thickness of convection zones in the two cases. Since GS98 models have deeper convection zone, the depletion of helium is lower. Thus the initial helium abundance of the 16 Cyg system is between 0.28 and 0.31. This is somewhat larger than the value found by Metcalfe et al. (2012) and close to the values found by Gruberbauer et al. (2013). The solar initial helium abundance was determined to be 0.278 ± 0.006 (Serenelli & Basu 2010). Thus our estimates of Y_0 for the 16 Cyg system is consistent with solar values particularly considering the fact that these stars have higher metallicity.

The fitted value of $\tau_{\rm He}$ obtained from observed frequencies for 16 Cyg B matched that obtained from fitting the model frequencies, but for 16 Cyg A the observed value is larger than that in all selected models. This could be due to some systematic errors in modelling or in the other observed quantities that were used to constrain the models.

The two sets of MESA models constructed with different heavy-element mixtures were used to check if the observed frequencies could distinguish between the different mixtures. For both sets of models, the value of Y, as well as $\tau_{\rm He}$ and $\tau_{\rm CZ}$ are very similar, although, as expected, there is a difference in the depth of the convection zone between the two sets with models constructed with the AGSS09 having a shallower convection zone depth and hence lower $\tau_{\rm CZ}$ than models with the GS98 mixture. But there is considerable overlap in

the range for each set of models. For 16 Cyg B the uncertainty in the value of τ_{CZ} obtained from observed frequencies is too large to distinguish between the two sets of models. For 16 Cyg A the error in τ_{CZ} from observed frequencies is reasonably small and if the systematic errors in modelling can be sorted out, it may be possible to use the models to distinguish between the two sets of models and get an independent handle on the controversy over the solar heavy-element abundance.

SB acknowledges support from NSF grant AST-1105930 and NASA grant NNX13AE70G. AM acknowledges support from he NIUS programme of HBCSE (TIFR). MJPFGM and JPF acknowledge support from the EC Project SPACEINN (FP7-SPACE-2012-312844) and JPF was also supported by the European Research Council (EC-FP7) through a fellowship of the Starting Grant ERC-2009-StG-239953. WJC acknowledges support from the UK Science and Technology Facilities Council (STFC). Funding for the Stellar Astrophysics Centre (SAC) is provided by The Danish National Research Foundation.

REFERENCES

Adelberger, E. G., Austin, S. M., Bahcall, J. N., et al. 1998, Reviews of Modern Physics, 70, 1265

Angulo, C., Arnould, M., Rayet, M., et al. 1999, Nuclear Physics A, 656, 3

Appourchaux, T., Chaplin, W. J., García, R. A., et al. 2012, A&A, 543, A54

Asplund, M., Grevesse, N., Sauval, A. J., Allende Prieto, C., & Kiselman, D. 2005, A&A, 435, 339

Asplund, M., Grevesse, N., Sauval, A. J., & Scott, P. 2009, ARA&A, 47, 481

Badnell, N. R., Bautista, M. A., Butler, K., et al. 2005, MNRAS, 360, 458

Bahcall, J. N., Basu, S., Pinsonneault, M., & Serenelli, A. M. 2005, ApJ, 618, 1049

Bahcall, J. N., Serenelli, A. M., & Basu, S. 2006, ApJS, 165, 400

Ballot, J., Turck-Chièze, S., & García, R. A. 2004, A&A, 423, 1051

Basu, S., & Antia, H. M. 1995, MNRAS, 276, 1402

—. 2008, Phys. Rep., 457, 217

—. 2013, Journal of Physics Conference Series, 440, 012017

Basu, S., Antia, H. M., & Narasimha, D. 1994, MNRAS, 267, 209

Basu, S., & Christensen-Dalsgaard, J. 1997, A&A, 322, L5

Basu, S., Mazumdar, A., Antia, H. M., & Demarque, P. 2004, MNRAS, 350, 277

Charbonneau, P. 1995, ApJS, 101, 309

Christensen-Dalsgaard, J., & Berthomieu, G. 1991, Theory of solar oscillations, ed. A. N. Cox, W. C. Livingston, & M. S. Matthews (Tucson, AZ: University of Arizona Press), 401–478

Christensen-Dalsgaard, J., di Mauro, M. P., Houdek, G., & Pijpers, F. 2009, A&A, 494, 205

Christensen-Dalsgaard, J., & Frandsen, S., eds. 1988, IAU Symposium, Vol. 123, Advances in helio- and asteroseismology; Proceedings of the Symposium, Aarhus, Denmark, July 7-11, 1986

Christensen-Dalsgaard, J., Thompson, M. J., & Gough, D. O. 1989, MNRAS, 238, 481

Cox, J., & Giuli, R. 1968, Principles of Stellar Structure: Physical principles, Principles of Stellar Structure No. v. 1 (Gordon and Breach)

Delahaye, F., & Pinsonneault, M. H. 2006, ApJ, 649, 529

Demarque, P., Guenther, D. B., Li, L. H., Mazumdar, A., & Straka, C. W. 2008, Ap&SS, 316, 31

Demarque, P., Woo, J.-H., Kim, Y.-C., & Yi, S. K. 2004, ApJS, 155, 667

Dotter, A., Chaboyer, B., Jevremović, D., et al. 2008, ApJS, 178, 89

Ferguson, J. W., Alexander, D. R., Allard, F., et al. 2005, ApJ, 623, 585

Formicola, A., Imbriani, G., Costantini, H., et al. 2004, Physics Letters B, 591, 61

García, R. A., Hekker, S., Stello, D., et al. 2011, MNRAS, 414, L6

Gough, D. O. 1990, in Lecture Notes in Physics, Berlin Springer Verlag, Vol. 367, Progress of Seismology of the Sun and Stars, ed. Y. Osaki & H. Shibahashi, 283

Gough, D. O., & Thompson, M. J. 1988, in IAU Symposium, Vol. 123, Advances in Helio- and Asteroseismology, ed. J. Christensen-Dalsgaard & S. Frandsen, 155

Grevesse, N., & Sauval, A. J. 1998, Space Sci. Rev., 85, 161

Gruberbauer, M., Guenther, D. B., MacLeod, K., & Kallinger, T. 2013, MNRAS, 435, 242

Houdek, G. 2004, in American Institute of Physics Conference Series, Vol. 731, Equation-of-State and Phase-Transition in Models of Ordinary Astrophysical Matter, ed. V. Celebonovic, D. Gough, & W. Däppen, 193–207

Houdek, G., & Gough, D. O. 2007, MNRAS, 375, 861

—. 2011, MNRAS, 418, 1217

Iglesias, C. A., & Rogers, F. J. 1996, ApJ, 464, 943

Imbriani, G., Costantini, H., Formicola, A., et al. 2005, European Physical Journal A, 25, 455

Kjeldsen, H., Bedding, T. R., & Christensen-Dalsgaard, J. 2008, ApJ, 683, L175

Kunz, R., Fey, M., Jaeger, M., et al. 2002, ApJ, 567, 643

Marigo, P., Girardi, L., Bressan, A., et al. 2008, A&A, 482, 883

Mathur, S., Metcalfe, T. S., Woitaszek, M., et al. 2012, ApJ, 749, 152

Mazumdar, A. 2005, A&A, 441, 1079

Mazumdar, A., & Antia, H. M. 2001, A&A, 377, 192

Mazumdar, A., Michel, E., Antia, H. M., & Deheuvels, S. 2011, in Transiting Planets, Vibrating Stars and Their Connection, ed. A. Baglin, M. Deleuil, E. Michel, C. Moutou, & T. Seman, Proceedings of Second *CoRoT* Symposium, 197

Mazumdar, A., Michel, E., Antia, H. M., & Deheuvels, S. 2012, A&A, 540, A31

Mazumdar, A., Monteiro, M. J. P. F. G., Ballot, J., et al. 2014, ApJ, 782, 18

Metcalfe, T. S., Monteiro, M. J. P. F. G., Thompson, M. J., et al. 2010, ApJ, 723, 1583

Metcalfe, T. S., Chaplin, W. J., Appourchaux, T., et al. 2012, ApJ, 748, L10

Miglio, A., Montalbán, J., Carrier, F., et al. 2010, A&A, 520, L6

Monteiro, M. J. P. F. G., Christensen-Dalsgaard, J., & Thompson, M. J. 1994, A&A, 283, 247

—. 2000, MNRAS, 316, 165

Monteiro, M. J. P. F. G., & Thompson, M. J. 1998, in IAU Symposium, Vol. 185, New Eyes to See Inside the Sun and Stars, ed. F.-L. Deubner, J. Christensen-Dalsgaard, & D. Kurtz, 317

Monteiro, M. J. P. F. G., & Thompson, M. J. 2005, MNRAS, 361, 1187

Paxton, B., Bildsten, L., Dotter, A., et al. 2011, ApJS, 192, 3

Peimbert, M., Luridiana, V., & Peimbert, A. 2007, ApJ, 666, 636

Piau, L., Ballot, J., & Turck-Chièze, S. 2005, A&A, 430, 571

Ramírez, I., Meléndez, J., & Asplund, M. 2009, A&A, 508, L17

Rogers, F. J., & Nayfonov, A. 2002, ApJ, 576, 1064

Roxburgh, I. W. 2011, in Transiting Planets, Vibrating Stars and Their Connection, ed. A. Baglin, M. Deleuil, E. Michel, C. Moutou, & T. Seman, Proceedings of Second *CoRoT* Symposium, 161

Roxburgh, I. W., & Vorontsov, S. V. 2003, A&A, 411, 215

Seaton, M. J. 2005, MNRAS, 362, L1

Serenelli, A. M., & Basu, S. 2010, ApJ, 719, 865

Silva Aguirre, V., Ballot, J., Serenelli, A. M., & Weiss, A. 2011, A&A, 529, A63

Street, J. O., Carroll, R. J., & Ruppert, D. 1988, The American Statistician, 42, 152

Thoul, A. A., Bahcall, J. N., & Loeb, A. 1994, ApJ, 421, 828

Turck-Chièze, S., Couvidat, S., Piau, L., et al. 2004, Physical Review Letters, 93, 211102

Vorontsov, S. V. 1988, in IAU Symposium, Vol. 123, Advances in Helio- and Asteroseismology, ed. J. Christensen-Dalsgaard & S. Frandsen, 151

White, T. R., Huber, D., Maestro, V., et al. 2013, MNRAS, 433, 1262

This manuscript was prepared with the AAS LaTeX macros v5.2.

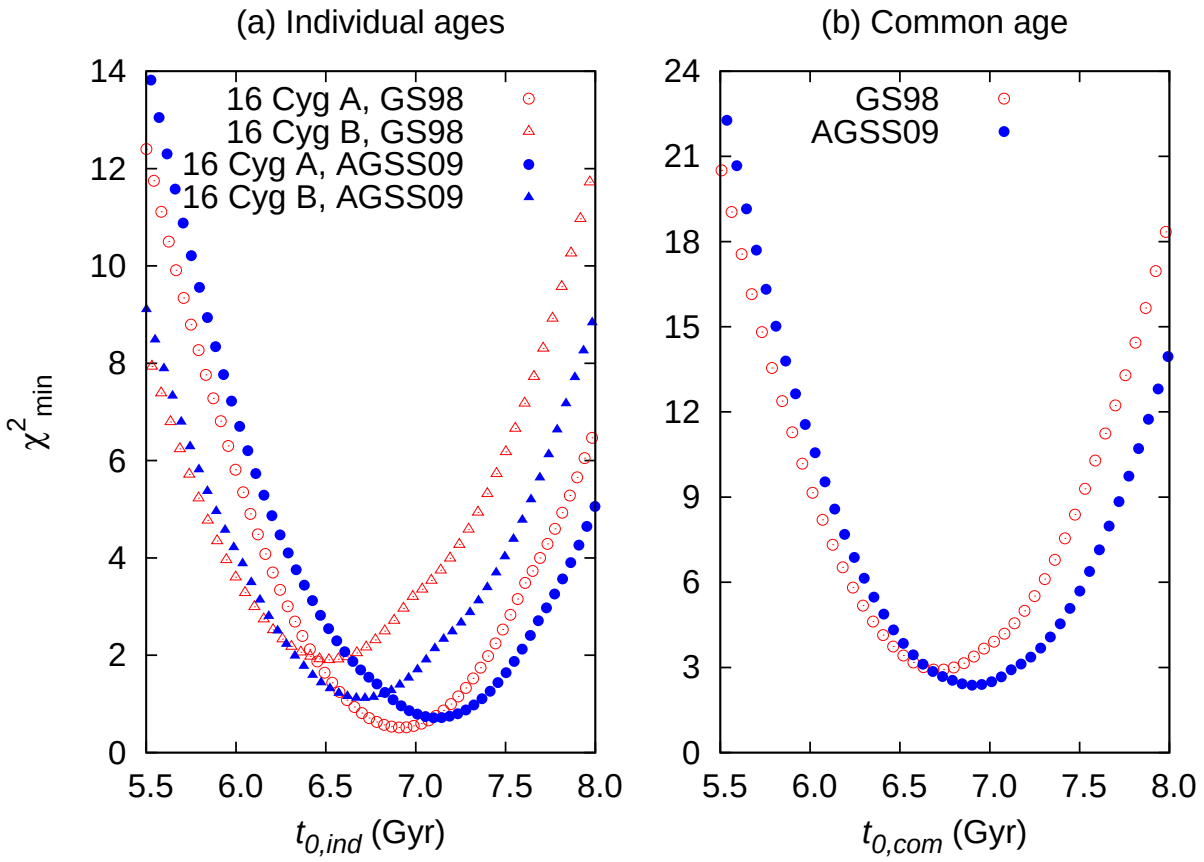

Fig. 1.— Selecting MESA models with appropriate age: (a) The four different types of points correspond to the four model ensembles of 16 Cyg A and B (two for a given star, with two metallicity mixtures). A point represents a model that minimizes the $\chi^2_{\rm ind}$, as defined in Eq. (8), at a given reference age $t_{0,\rm ind}$. (b) The two different types of points correspond to the two model ensembles of 16 Cyg system with two metallicity mixtures. A point represents a pair of models, one from the model ensemble of 16 Cyg A and the other from 16 Cyg B that minimizes the $\chi^2_{\rm com}$, as defined in Eq. (9), at a given reference common age $t_{0,\rm com}$.

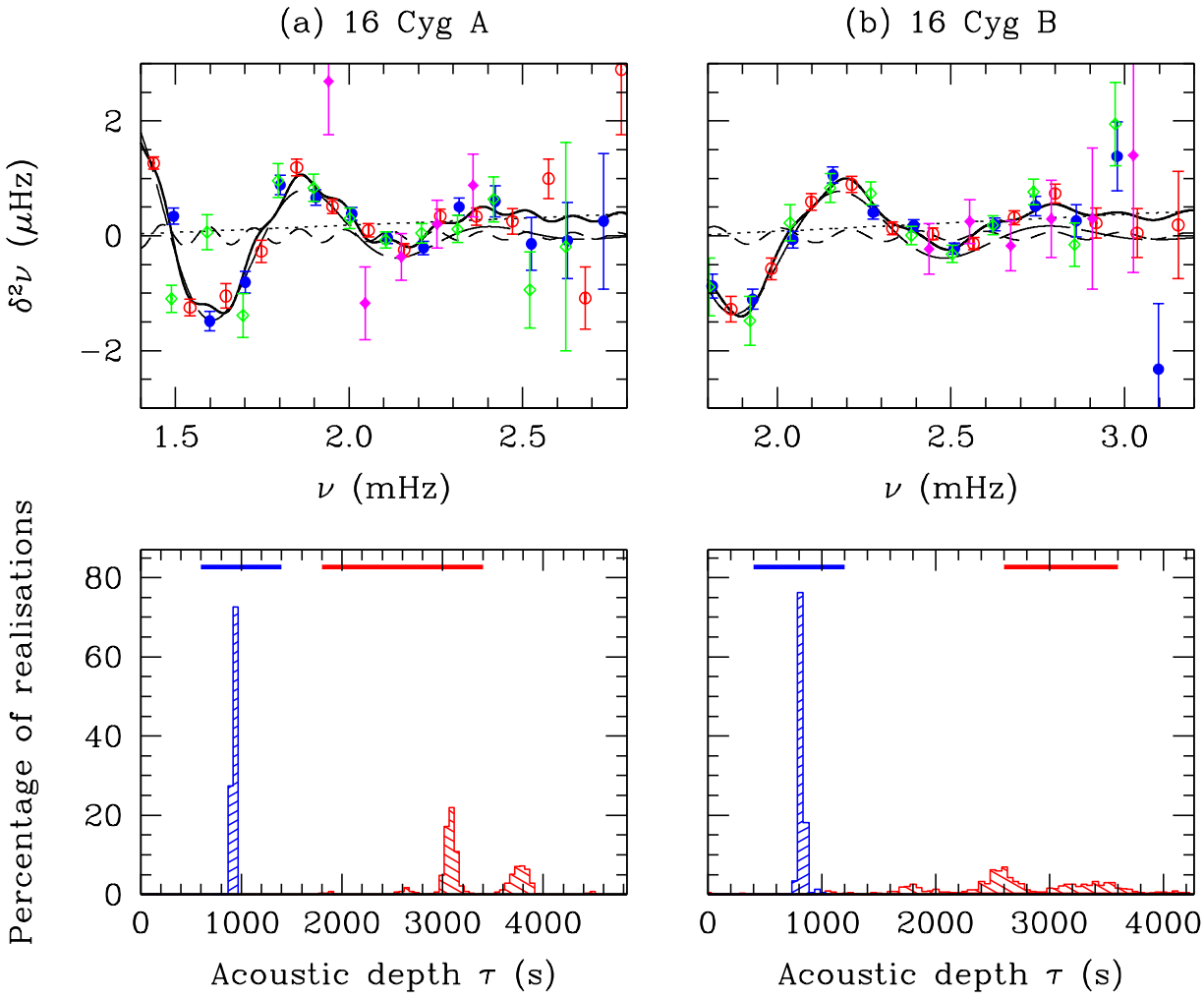

Fig. 2.— Fit to the second differences (Method A) for 16 Cyg A and B. The upper panels show the fits (solid line) as well as the three components on the RHS of Eq. (3). The dotted line shows the smooth part, the short-dashed line shows the contribution from CZ signal and the long-dashed line shows the contribution from the HeII ionization zone signal. The blue filled circles are the second differences for $l = 0$ modes, the red open circles are for $l = 1$, the green open diamonds are for $l = 2$, and the magenta filled diamonds are for $l = 3$. The lower panels show the histograms of distribution of $\tau_{\rm He}$ (blue) and $\tau_{\rm CZ}$ (red). The horizontal bars at the top show the range of initial guesses for the two parameters used for fitting.

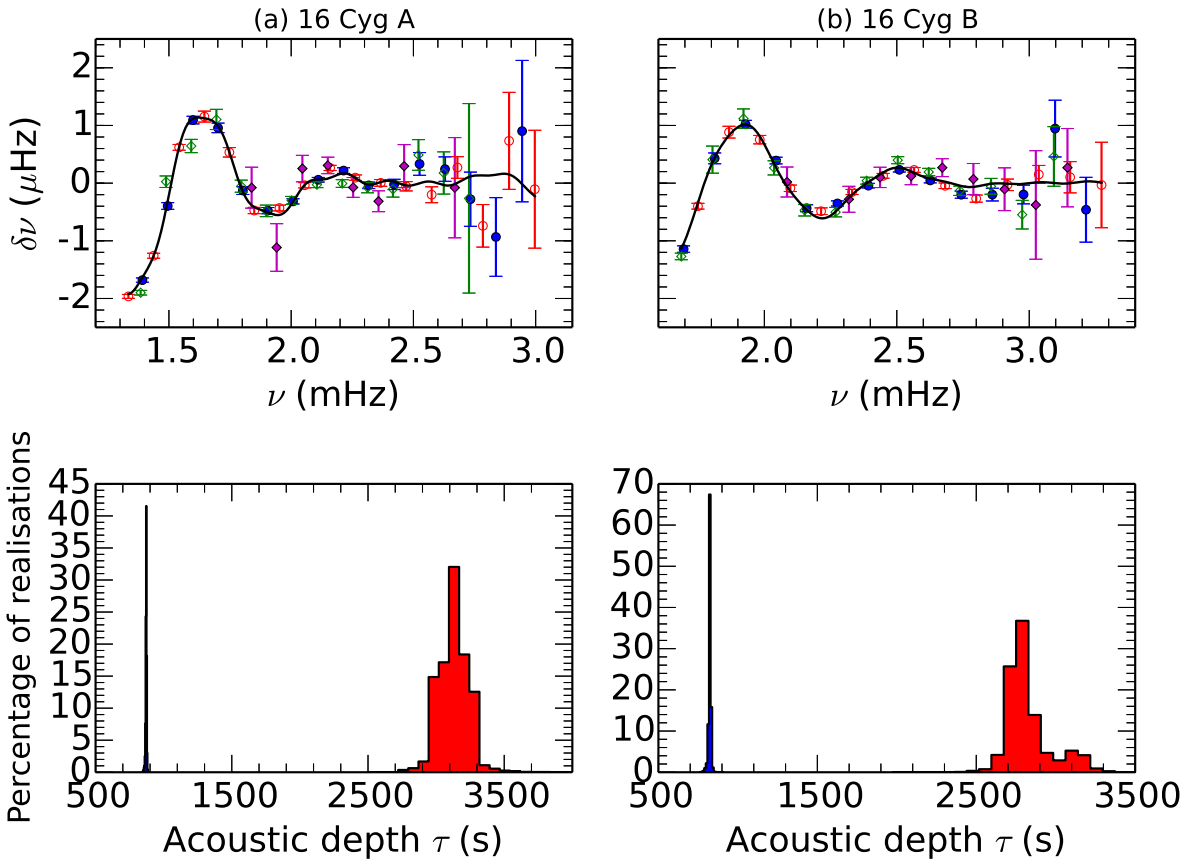

Fig. 3.— Fit to the frequencies (Method B) for 16 Cyg A and B. The upper panels show the fit (solid line) to Eq. (4). The symbols are same as in Fig. 2. The lower panels show the histograms of distribution of $\tau_{\rm He}$ (blue) and $\tau_{\rm CZ}$ (red).

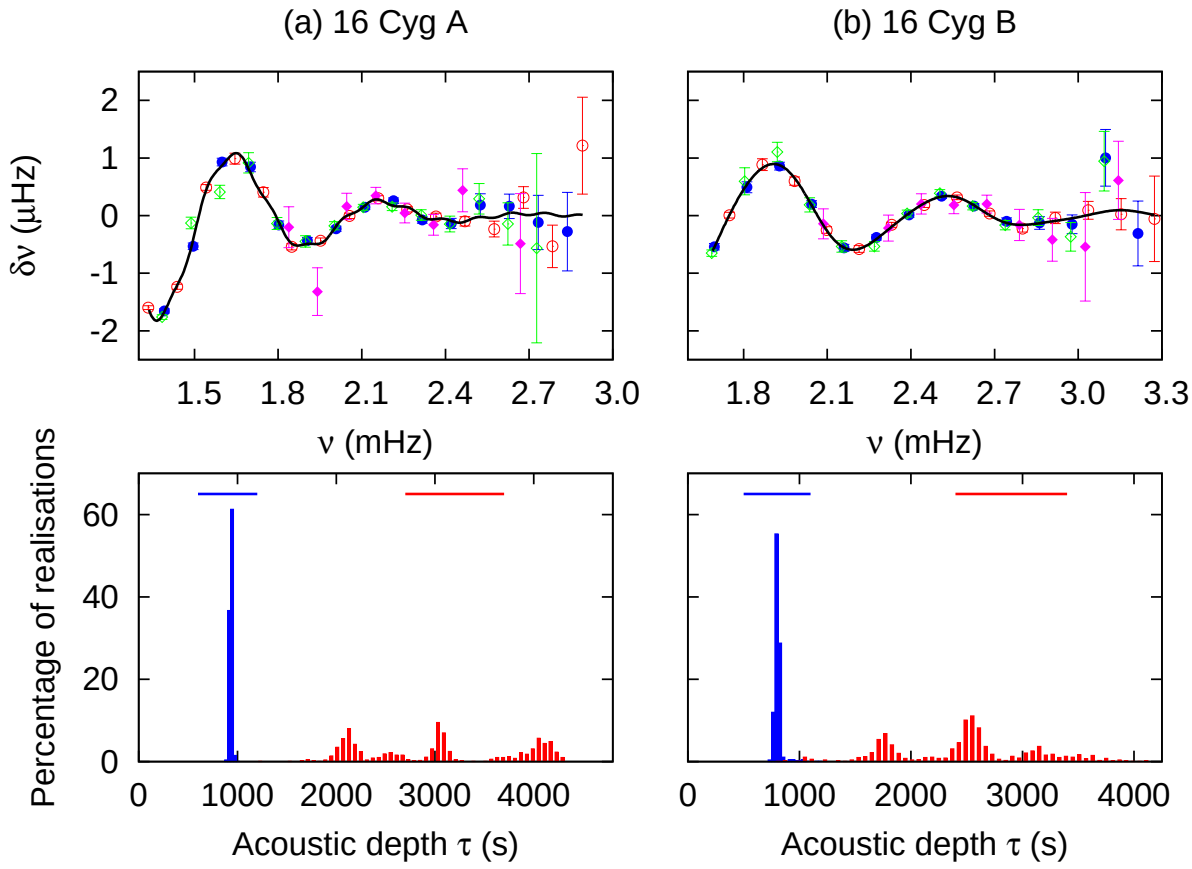

Fig. 4.— Fit to the frequencies (Method C) for 16 Cyg A and B. The upper panels show the combined oscillatory signal obtained by removing the contribution of the polynomial $P_{l,\mathrm{C}}(n)$ from the frequencies. The symbols are same as in Fig. 2. The curve shows $f(n,l)$ without the contribution of $P_{l,\mathrm{C}}(n)$. The lower panels show the histograms of distribution of τ_{He} (blue) and τ_{CZ} (red). The horizontal bars at the top show the range of initial guesses for the two parameters used for fitting.

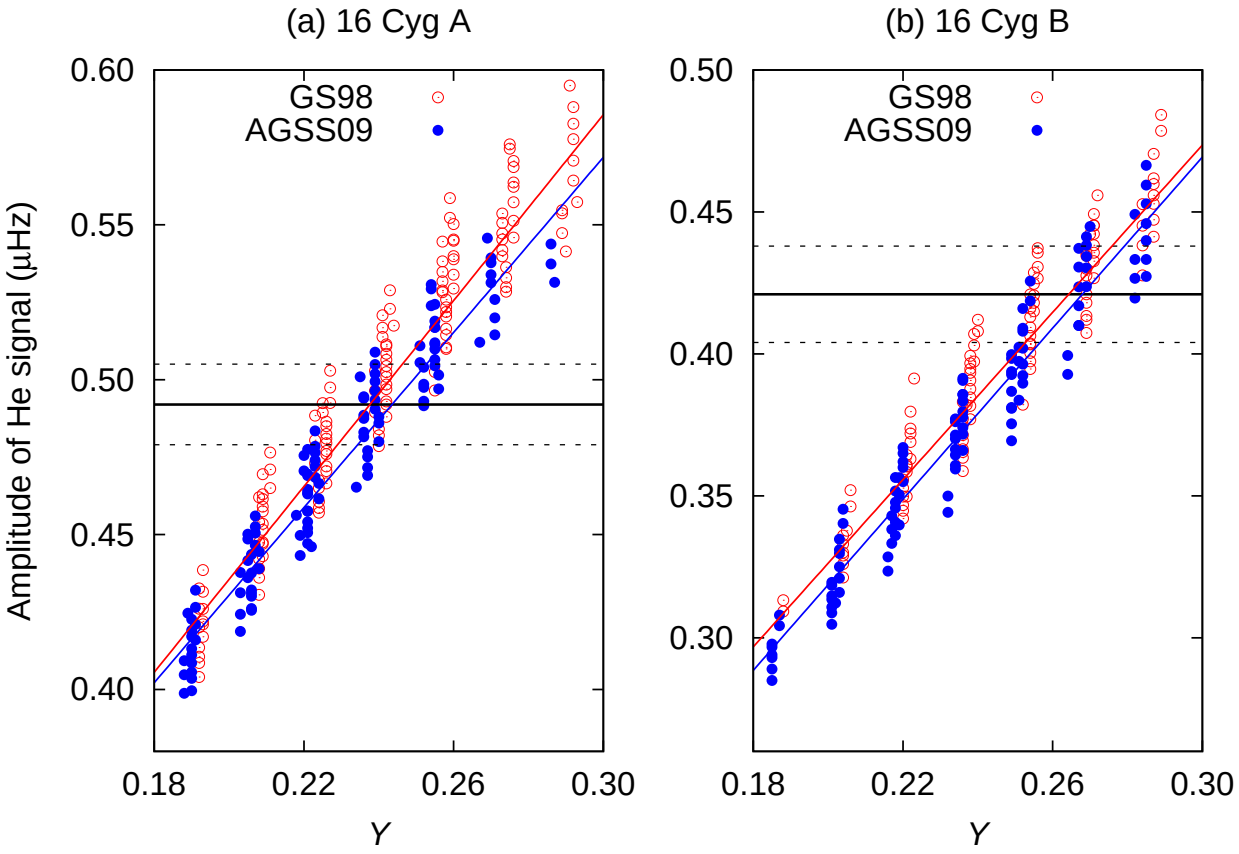

Fig. 5.— Amplitude of the helium signal obtained using Method A as a function of Y for 16 Cyg A and B. The continuous horizontal line is the observed amplitude, with the dashed lines representing the 1σ uncertainty limits. The points are the results for the MESA models, while the red and blue lines show the straight line fit to these points.

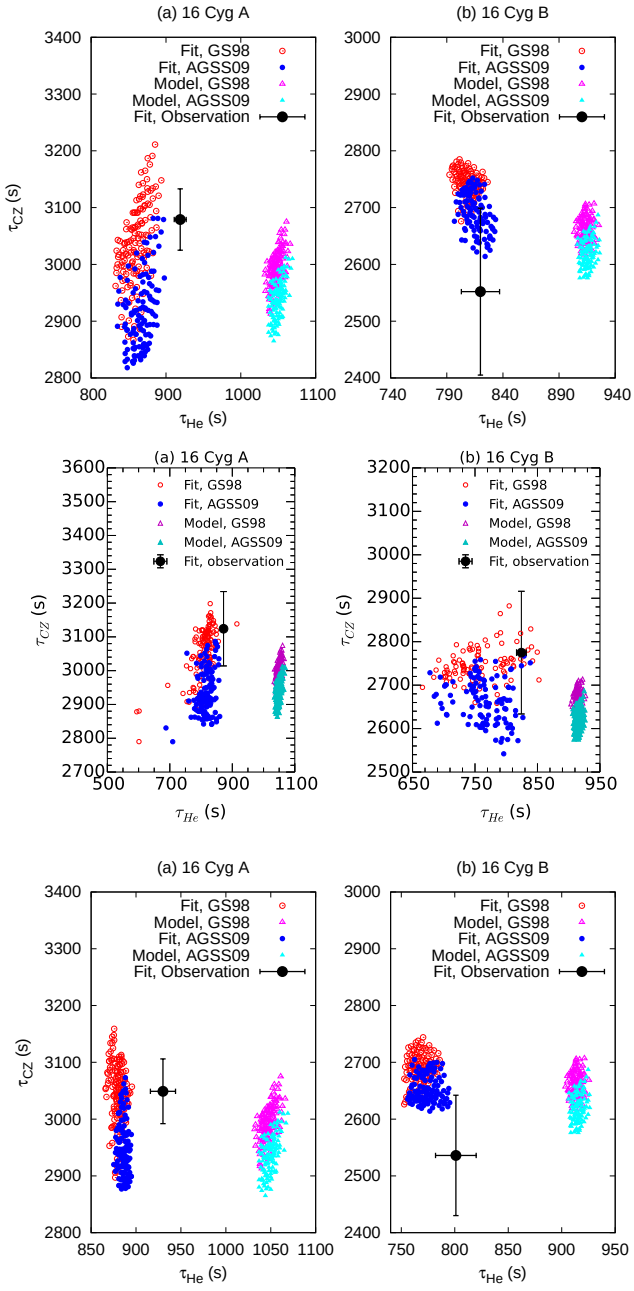

Fig. 6.— Comparing $\tau_{\rm He}$ and $\tau_{\rm CZ}$ for (a) 16 Cyg A and (b) 16 Cyg B. The black point with error-bars represent the observations. Other points represent the τ values for the MESA models. The top panels show the results using Method A, the middle panels show those using Method B and the bottom panels show the same using Method C.

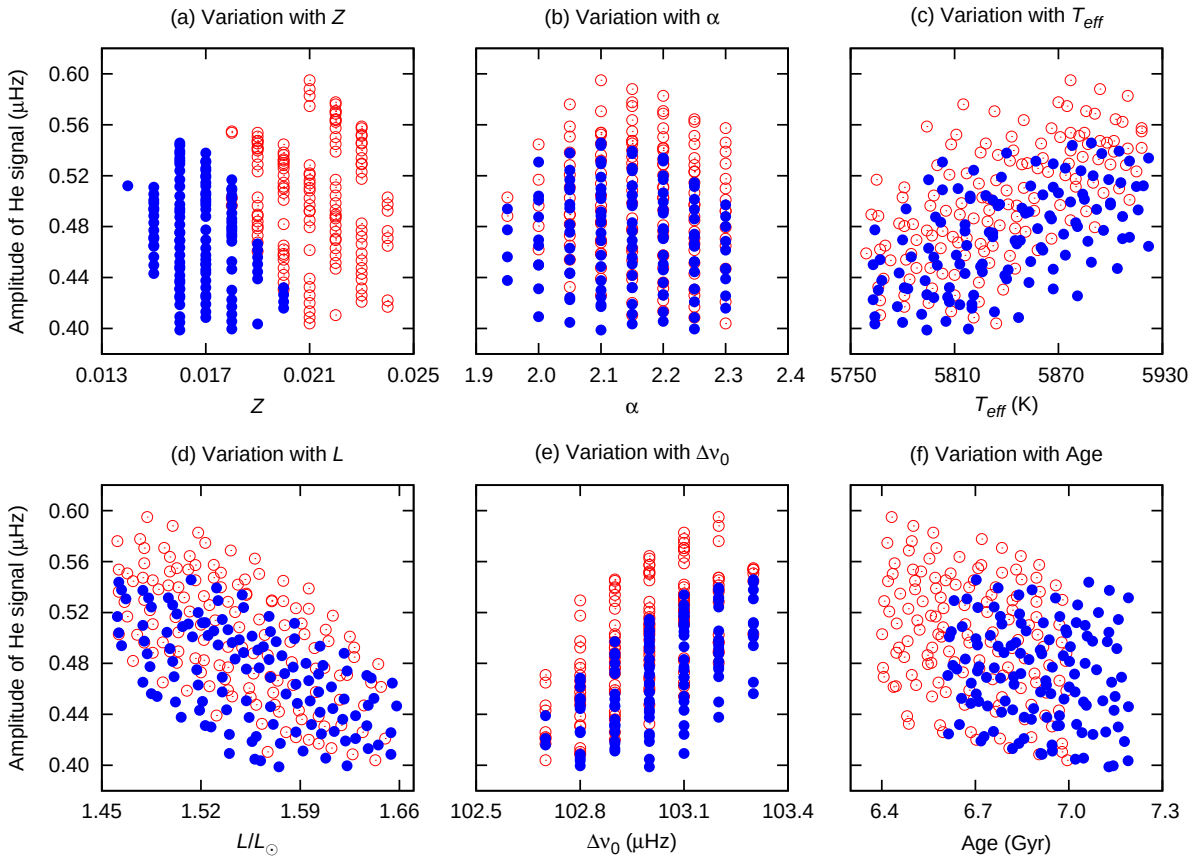

Fig. 7.— The variation of the average amplitude of the helium signal as a function of different model parameters. Results are shown for 16 Cyg A MESA models and amplitudes are calculated using Method A. Models with both GS98 (red open circles) and AGSS09 (blue filled circles) heavy-element mixtures are shown.

Table 1. Various observables used to constrain the models of 16 Cyg A and B.

Observable	16 Cyg A	16 Cyg B	Reference
$T_{\rm eff}$	5839±42 K	5809±39 K	1
$\log g$	4.29±0.02 dex	4.36±0.02 dex	1
L	1.56±0.05 $L_\odot$	1.27±0.04 $L_\odot$	2
[Fe/H]	0.096±0.040 dex	0.096±0.040 dex	3
Δ_0	102.9±0.2 μHz	116.5±0.2 μHz	···
$\langle d_{02} \rangle$	5.82±0.03 μHz	6.70±0.03 μHz	···

Note. — Surface [Fe/H] is assumed to be same for both components with increased uncertainty. Average large and small separations were calculated using observed frequencies.

References. — (1) White et al. (2013); (2) Metcalfe et al. (2012); (3) Ramírez et al. (2009)

Table 2. Observed oscillation frequencies for 16 Cyg A and B.

	16 Cyg A				16 Cyg B			
n	$l = 0$ (μHz)	$l = 1$ (μHz)	$l = 2$ (μHz)	$l = 3$ (μHz)	$l = 0$ (μHz)	$l = 1$ (μHz)	$l = 2$ (μHz)	$l = 3$ (μHz)
11	...	1334.392±0.034	1384.368±0.040	...	...	...	...	...
12	1391.639±0.037	1437.520±0.043	1488.353±0.100	...	...	...	1686.327±0.057	...
13	1494.996±0.058	1541.914±0.050	1591.242±0.115	...	1695.066±0.056	1749.184±0.050	1804.197±0.235	...
14	1598.695±0.066	1645.058±0.095	1694.193±0.175	...	1812.420±0.094	1866.525±0.102	1921.176±0.168	...
15	1700.909±0.083	1747.154±0.082	1795.757±0.105	1838.283±0.355	1928.900±0.068	1982.587±0.073	2036.677±0.123	2085.517±0.260
16	1802.316±0.068	1848.980±0.054	1898.284±0.100	1940.756±0.413	2044.274±0.058	2098.076±0.056	2152.405±0.100	...
17	1904.611±0.054	1951.997±0.050	2001.647±0.070	2045.922±0.229	2159.580±0.060	2214.159±0.058	2268.966±0.082	2319.208±0.225
18	2007.572±0.045	2055.527±0.046	2105.314±0.051	2149.914±0.143	2275.946±0.045	2331.138±0.044	2386.267±0.060	2436.792±0.176
19	2110.915±0.040	2159.153±0.045	2208.907±0.067	2253.539±0.172	2392.718±0.040	2448.250±0.042	2503.575±0.061	2554.149±0.150
20	2214.226±0.049	2262.536±0.047	2312.545±0.091	2357.368±0.181	2509.668±0.038	2565.398±0.042	2620.566±0.064	2671.754±0.155
21	2317.326±0.056	2366.260±0.059	2416.301±0.137	2462.077±0.373	2626.399±0.042	2682.409±0.048	2737.741±0.081	2789.187±0.270
22	2420.931±0.089	2470.322±0.081	2520.695±0.266	...	2743.327±0.061	2799.735±0.062	2855.682±0.137	2906.915±0.371
23	2525.141±0.197	2574.639±0.138	2624.147±0.366	2669.376±0.869	2860.773±0.110	2917.799±0.100	2973.470±0.248	3024.940±0.941
24	2629.212±0.212	2679.951±0.188	2727.410±1.643	...	2978.481±0.162	3036.084±0.156	3093.204±0.517	3144.365±0.679
25	2733.199±0.470	2784.178±0.369	...	...	3097.575±0.492	3154.418±0.271	...	...
26	2837.442±0.682	2891.303±0.841	...	...	3214.348±0.562	3272.941±0.741	...	...
27	2944.587±1.226	2996.533±1.022	...	...	...	...	...	...

Table 3. Physical parameters obtained by fitting the observed frequencies of 16 Cyg A and B.

Method	Amplitude of CZ Signal (μHz)	$\tau_{\rm CZ}$ (s)	Amplitude of He Signal (μHz)	$\tau_{\rm He}$ (s)
		16 Cyg A		
A	0.072 ± 0.011	3079 ± 54	0.492 ± 0.013	919 ± 9
B	0.030 ± 0.012	3124 ± 110	0.435 ± 0.036	872 ± 4
C	0.055 ± 0.012	3049 ± 57	0.508 ± 0.017	930 ± 14
		16 Cyg B		
A	0.043 ± 0.010	2552 ± 147	0.421 ± 0.017	820 ± 17
B	0.048 ± 0.018	2775 ± 141	0.900 ± 0.031	824 ± 8
C	0.044 ± 0.012	2536 ± 106	0.449 ± 0.018	801 ± 19

Table 4. Helium abundances of 16 Cyg A and B.

Method	MESA		YREC
	GS98	AGSS09	GS98
	16 Cyg A		
A	0.238 ± 0.009	0.243 ± 0.009	0.231 ± 0.009
B	0.239 ± 0.021	0.242 ± 0.023	0.236 ± 0.016
C	0.250 ± 0.009	0.251 ± 0.009	0.249 ± 0.009
	16 Cyg B		
A	0.263 ± 0.012	0.266 ± 0.012	0.257 ± 0.009
B	0.218 ± 0.013	0.228 ± 0.011	0.219 ± 0.009
C	0.251 ± 0.010	0.254 ± 0.010	0.255 ± 0.009